Monolayers in Three Dimensions: NMR, SAXS, Thermal, and Electron Hopping Studies of Alkanethiol Stabilized Gold Clusters

Roger H. Terrill,[†] Timothy A. Postlethwaite,[‡] Chun-hsien Chen,[§] Chi-Duen Poon, Andreas Terzis, Aidi Chen, James E. Hutchison,[⊥] Michael R. Clark, George Wignall,[∥] Juan D. Londono,[∥] Richard Superfine,[#] Mike Falvo,[#] Charles S. Johnson Jr.,* Edward T. Samulski,* and Royce W. Murray*

Contribution from the Kenan Laboratories of Chemistry and Department of Physics and Astronomy, University of North Carolina, Chapel Hill, North Carolina 27599-3290, and Oak Ridge National Laboratories, P.O. Box 2008, Oak Ridge, Tennessee 37831-6393

Received July 20, 1995[⊗]

Abstract: Gold clusters stabilized by chemisorbed monolayers of octane-, dodecane- or hexadecanethiolate have been investigated in solution and in the solid phase. These materials can be pumped free of solvent to form a dark brown solid that can be re-dissolved in nonpolar solvents. Their exceptional stability suggests they be viewed as *cluster compounds*. The self-assembled alkanethiolate monolayers stabilizing the metal clusters can be investigated using techniques that are insufficiently sensitive for study of a monolayer on a flat surface, e.g., ^{1}H and ^{13}C NMR, elemental analysis, differential scanning calorimetry (DSC), thermogravimetry (TGA), and diffusion-ordered NMR spectroscopy (DOSY). Results from such measurements, combined with small-angle X-ray scattering (SAXS) data on solutions of the clusters and images from scanning tunneling (STM), and atomic force microscopy (AFM), are consistent with a small, monodisperse (12 Å radius) gold core, which modeled as a sphere contains ~400 Au atoms and ~126 alkanethiolate chains, or if modeled as a cuboctahedral structure contains 309 Au atoms and ~95 alkanethiolate chains. High-resolution NMR spectra of cluster solutions display well-defined resonances except for methylenes nearest the gold interface; the absence of the latter resonances is attributed to a combination of broadening mechanisms based on the discontinuous change in magnetic susceptibility at the metal−hydrocarbon interface and residual dipolar interactions. Films of the dry, solid cluster compound on interdigitated array electrodes exhibit current−potential responses characteristic of electron hopping conductivity in which electrons tunnel from Au core to Au core. The electron hopping rate decreases and the activation barrier increases systematically at longer alkane chain length. The results are consistent with electron transport rate control being a combination of thermally activated electron transfer to create oppositely charged Au cores (cermet theory) and distance-dependent tunneling (β = 1.2 Å^{-1}) through the oriented alkanethiolate layers separating them.

The self-organization of alkanethiols chemisorbed on planar Au surfaces has generated intense interest in understanding its chemical basis.[1] The two-dimensional character of self-assembled monolayers places limits, however, on the experiments by which they can be probed when they are chemisorbed on planar Au surfaces, e.g.,[1] wetting, helium diffraction, scanning probe, interfacial electron transfers, FTIR spectroscopy, etc. An important recent report[2] describing the stabilization of Au colloids with chemisorbed C_{12} alkanethiol opens the way to study of two-dimensional monolayers by additional conventional (i.e., three dimensional) methodologies such as NMR spectroscopy, thermal methods, and electronic conductance. The alkanethiol-stabilized Au colloids can be pumped free of solvent after their preparation, and reversibly redissolved in hydrophobic solvents. Their exceptional stability suggests that they be viewed as cluster compounds; they are in fact rather stable compared to other known[3] ligand-stabilized metal clusters. The large quantity of alkanethiol monolayer stabilizing the dissolved metal clusters facilitates their study in solutions as well as in bulk samples of clusters, problems of measurement sensitivity being greatly lessened. At the same time, the possibility arises that the character of alkane chain ordering on the periphery of the nanoparticles may exhibit intrinsic differences (owing to the surface curvature, its possible presentation of variable crystal facets, and the manner of self-assembly) from monolayers formed on well-defined, planar, Au(111) surfaces.[1]

* Address correspondence to this author at the University of North Carolina.
[†] Department of Chemistry, University of Illinois, Urbana, IL.
[‡] W. R. Grace and Co, Washington Research Center, 7379 Route 32, Columbia, MD 21044-4098.
[§] Department of Chemistry, National Sun Yat-Sen University, Kaohsiung, Taiwan 804, ROC.
[⊥] Department of Chemistry, University of Oregon, Eugene, OR97403-1253.
[∥] Oak Ridge National Laboratories.
[#] Department of Physics and Astronomy. University of North Carolina.
[⊗] Abstract published in *Advance ACS Abstracts,* December 1, 1995.

(1) (a) DuBois L. H.; Nuzzo, R. G. *Annu. Rev. Chem. Phys.* **1992**, *43*, 437. (b) Laibinis, P. E.; Whitesides, G. M.; Allara D. L.; Tao, Y.-T.; Parikh, A. N.; Nuzzo, R. G. *J. Am. Chem. Soc.* **1991**, *133*, 7152. (c) Chidsey, C. E. D.; Liu, G.; Scoles, G.; Wang, J. *Langmuir*, **1990**, *6*, 1804. (d) Fenter, P.; Eisenberger, P.; Liang, K. S. *Phys. Rev. Lett.* **1993**, *70*, 2447. (e) Chidsey, C. E. D. *Science* **1991**, *251*, 919. (f) Chailapakul, O.; Sun, L.; Xu C.; Crooks, R. M. *J. Am. Chem. Soc.* **1993**, *115*, 12439. (g) Nemetz, A; Fischer T.; Ulman, A.; Knoll, W. *J. Chem. Phys.* **1993**, 987. (h) Schneider, T. W.; Buttry, D. A. *J. Am. Chem. Soc.* **1993**, *115*, 12391. (i) Widrig, C. A.; Alves, C. A.; Porter, M. D. *J. Am. Chem. Soc.* **1991**, *113*, 2805. (j) Kim, Y.-T.; McCarley, R. L.; Bard A. J. *J. Phys. Chem.* **1992**, *96*, 7416.

(2) Brust, M.; Walker, M.; Bethell, D.; Schriffin, D. J.; Whyman, R. *J. Chem. Soc., Chem. Commun.* **1994**, 801.

(3) (a) Schmid, G. *Chem. Rev.* **1992**, *92*, 1709. (b) Schmid, G., Ed. *Clusters and Colloids, From Theory to Applications*; VCH: Weinheim, 1994. (c) Peschel, S.; Schmid, G. *Angew. Chem. Int. Ed. Engl.* **1995**, *34*, 1442. (d) Duteil, A.; Schmid, G. *J. Chem. Soc., Chem. Commun.* **1995**, 31. (e) Schmid, G.; Hess, H. *Z. Anorg. Allg. Chem.* **1995**, *621*, 147.

0002-7863/95/1517-12537$09.00/0

This paper introduces new measurements of alkanethiol monolayers on Au clusters stabilized by alkanethiols of varying chain length (8, 12, and 16 carbons). (For brevity, they will be referred to as C_8, C_{12}, and C_{16} clusters.) In carbon NMR spectra of dilute cluster solutions, the methyl and outermost methylene units in the alkanethiol chains display sharp resonances, while those proximate to the gold (α, β, and γ methylenes) are not seen. A physical model is presented to account for this unusual observation. Differential scanning calorimetry and thermogravimetry of pure, solvent-free cluster compounds reveals melting transitions for clusters stabilized by C_{12} and C_{16} alkanethiol monolayers and well-defined thermal decompositions of the organic monolayers, respectively. The current–potential electronic conductivity responses of films of solvent-free cluster compounds on interdigitated array electrodes are characteristic of electron hopping; their analysis yields approximate rate constants, electronic coupling coefficients, and activation barriers for electron tunneling between the Au cores through intervening alkanethiol layers of various chain length. Observations with SAXS,[4] DOSY,[5] STM, and AFM give information about the sizes of the cluster compounds and their Au cores.

Experimental Section

Chemicals. Hydrogen tetrachloroaurate (Strem, 99.99%), octanethiol (Aldrich, 97%), dodecanethiol (Aldrich, 98%), hexadecylmercaptan (Aldrich, 92%), sodium borohydride (Johnson Matthey 98%), tetraoctylammonium bromide (Aldrich, 98%), toluene (Burdick and Jackson HPLC grade), methylene chloride (Mallinkrodt, spectrophotometric grade), and ethanol (AAPER, absolute) were used as received.

Synthesis. Octane, dodecane, and hexadecanethiol derivatized gold colloids were synthesized as described by Brust et al.[2a] for the C_{12} variety, using the C_8 and C_{16} alkanethiols in analogous stoichiometric proportion. Briefly, hydrogen tetrachloroaurate (aq) is extracted into toluene and metathesized to the tetraoctylammonium salt with a toluene solution of tetraoctylammonium bromide. To this toluene solution is added an equimolar amount of alkanethiol, followed by an aqueous solution of sodium borohydride. Reduction of the gold salt and concomitant derivatization by alkanethiol is evidenced by prompt darkening of the toluene phase. After the solution was stirred for 2 h, the toluene layer was separated, reduced to *ca.* 20 mL, and poured into 1 L of ethanol, where flocculation slowly ensued. Flocculation was carried out twice at 0 °C overnight for the C_8 and C_{12} materials, and for *ca.* 36 h for the more slowly aggregating C_{16} variety. Cluster compound samples and solutions are generally quite stable except that some surfaces, i.e., certain brands of NMR tubes (both in and out of the magnet), Pasteur pipet tips, and glass wool provoked their decomposition with formation of Au metal films on the surfaces.

Elemental Analyses. Elemental analyses of the cluster compounds for C, H, S, and Au (Galbraith) were respectively as follows. C_8: 13.72, 2.46, 4.49, 74.79%. C_{12}: 18.24, 3.29, 4.16, 68.78%. C_{16}: 25.61, 4.58, 4.28, 65.34%. Expressed as atomic percentages in the (CHS) fraction, these analytical results are the following. C_8 cluster: calcd, C = 66.14, H = 11.79, S = 22.07; found, C = 66.38, H = 11.90, S = 21.72. C_{12} cluster: calcd, C = 71.64, H = 12.44, S = 15.92; found, C = 74.3, H = 13.29, S = 12.42.

Density Measurements. Cluster compound films of ~0.1 mg were drop cast from hexane solution onto carefully tared (Cahn 120 Electrobalance) glass coverslips and dried to constant weight in air. Eight to twelve profilometric traces (Tencor AlphaStep 100 Profilometer) of the film were digitized and averaged together to calculate film area and volume. The films are sufficiently hard that tracking (gouging) by the profilometer tip did not occur.

NMR and Diffusion Measurements. High-resolution ^1H and ^{13}C NMR spectra were obtained using a Bruker AMX-300 spectrometer with 5 mm triple resonance and inverse detection probes. Solutions were prepared in $CDCl_3$ and all measurements were conducted at room temperature. The diffusion-ordered NMR (DOSY) experiment has been described in detail elsewhere.[5a,b] Instrumentation for high-performance pulsed field gradient NMR (PFG-NMR) consists of a Bruker AC-250 spectrometer with custom-built 10 mm probes (coil constants 0.175 and 0.156 T m^{-1} A^{-1}) and computer-controlled gradient drivers. The LED pulse sequence[5c] was employed with a constant diffusion time (Δ = 525 ms), and 30–40 free induction decays (FID's), each associated with a different value of gradient area (q) ranging from 1.7 × 10^4 to 7.5 × 10^5 m^{-1}, were collected in each experiment. The cluster compound sample concentrations were the following: 70 mg/mL C_8 in $CDCl_3$; 50 mg/mL C_{12} in CD_2Cl_2; and 50 mg/mL C_{16} in $CDCl_3$, in standard 5 mm NMR tubes. In all experiments, the probe temperature was maintained at 295 ± 1 K.

Thermal Analysis. Differential scanning calorimetry (DSC) and thermogravimetry (TGA) were performed with a Seiko SSC 5200 thermal analysis system. For DSC and TGA, 10–30 mg of accurately weighed samples of extensively dried (vacuum, room temperature) cluster compound were analyzed in N_2 atmosphere in standard (crimped, DSC) aluminum pans. Cooling and heating DSC scans were recorded for samples between +100 and −100 °C (6 °C/min). Some hysteresis was evident in the broad DSC peaks despite the *ca.* 15 min holding time at the starting temperature. TGA runs were recorded from 30 to 600 °C at 20 °C/min.

STM and AFM. Scanning tunneling microscopy (STM) was done with a Nanoscope II STM (Digital Instruments, Santa Barbara, CA) and mechanically cut Pt/Ir tunneling tips operating in the constant-current mode. STM images were calibrated by imaging HOPG (highly oriented pyrolytic graphite) in air. The samples for STM measurements were prepared by placing 10 μL of cluster solution (1-mg cluster in 1 mL of dichloromethane) on fresh-cleaved HOPG substrates and allowing the solvent to evaporate. Tapping-mode atomic force microscopy (AFM) was done with a Nanoscope III (Digital Instruments, Santa Barbara, CA) on identically prepared substrates. AFM image height was calibrated by using the AFM to measure lattice plane steps in an etched muscovite mica sample.[7]

IDA Electrodes. Interdigitated array (IDA) electrodes consisting of 100 (n_f) interlocking 3 μm wide, 2 mm long (l), and 0.1 μm thick (h) gold or platinum film fingers separated by 5-μm gaps, generously donated by Nippon Telephone and Telegraph, were patterned on Si/SiO_2 substrates with an insulating Si_3N_4 overlayer surrounding the electrode pattern. Electrodes were cleaned by rinsing in toluene and methylene chloride followed by a brief Ar plasma cleaning (*ca.* 16 W, 200 mTorr Ar flowing, 90 s). Prior to film casting, both sets of IDA fingers were independently made working electrodes in an electrochemical cell, and the chemical reversibility of the aqueous $[Fe(CN)_6]^{3-/4-}$ couple was analyzed by cyclic voltammetry to confirm the macroscopic IDA area and the electrochemical activity of the platinum fingers; voltammetric peak separations were within ~20 mV of the ideal value of 59 mV. The clean, film-free IDA electrodes exhibited typically less than 1 pA/V leakage in vacuum. The cross-sectional area of the parallel plate polymer sandwich (A) is taken as the area of the IDA finger walls facing each other, $A = (n_f - 1)lh$.

Cluster Film Preparation and Electrical Conductivity Measurement. Films of C_8, C_{12}, and C_{16} clusters were prepared for electrical conductivity measurements by drop-casting 2.5 to 15 μL of toluene or methylene chloride solutions containing 100 mg/mL concentrations onto IDA electrodes. The film thicknesses, measured with a Tencor AlphaStep 100 profilometer in most cases, were between 2 and 20 μm and generally uniform over the IDA finger arrays. Film-to-film thickness variations were 30–50%. Current–voltage responses were taken under vacuum (<50 mTorr) on well-dried films at controlled temperatures. Temperature control was achieved with either a Lakeshore Cryonics Model 330 temperature controller and Janis Model C21-TR He cryostat or with a stage of local construction heated by a 60W Omega Kapton

(4) (a) Hendricks, R. W. *J. Appl. Phys.*, **1978**, 11, 15. (b) Wignall, G. D.; Lin, J. S.; Spooner, S. *J. Appl. Crystallogr.* **1990**, *23*, 241. (c) Russell, T. P.; Lin, J. S.; Spooner, S.; Wignall G. D. *J. Appl. Crystallogr.* **1988**, *21*, 629. (d) Guinier, A.; Fournet, G. *Small Angle Scattering of X-Rays*; John Wiley: New York, 1955. (e) Wignall, G. D. *Neutron and X-Ray Scattering, Polymer Properties Handbook;* Mark, J. E., Ed.; American Institute of Physics, in press. (f) Wignall, G. D.; Bates, F. S. *J. Appl. Crystallogr.* **1986**, *20*, 28. (g) Hayter, J. B.; Penfold, J. *Colloid Polym. Sci.* **1983**, *261*, 1022.

(5) (a) Morris, K. F.; Johnson, C. S., Jr. *J. Am. Chem. Soc.* **1993**, *115*, 4291. (b) Hinton, D. P.; Johnson, C. S., Jr. *J. Phys. Chem.* **1993**, *97*, 9064. (c) Gibbs, S. J.; Johnson, C. S., Jr. *J. Magn. Reson.* **1991**, *93*, 395. (d) Provencher, S. W. *Comput. Phys. Commun.* **1982**, *27*, 213. (e) Provencher, S. W. *Comput. Phys. Commun.* **1982**, *27*, 229.

strip heater powered by the 110 V triac output of an Omega CN76000 two-channel temperature controller with below-ambient temperature control achieved by circulating L_{N2}-cooled N_2 through copper coils contacting the stage bottom, controlling the N_2 flow with the second channel of the temperature controller. Potential sweep and step waveforms were synthesized, and the current signals (converted to voltage by a circuit of local construction) digitized by a DATEL-412 analog IO board in an IBM compatible PC using locally written software. High-field *I/V* plots were obtained by placing a Kepco BOP 100−1M operational power supply-10× amplifier in line with the excitation signal. AC impedance spectra were acquired with either a EG&G-Princeton Applied Research Model 273 potentiostat and Model 5210EC lock-in amplifier or a Schlumberger Model 1286 potentiostat/1255 frequency response analyzer operating under computer control and using commercial data acquisition software.

Small-Angle X-ray Scattering (SAXS). The experiments were performed on cluster solutions on the Oak Ridge National Laboratory 10 m SAXS instrument,[4a,b] with a sample−detector distance of 1.069 m using Cu Kα radiation ($\lambda = 1.54$ Å) and a 20 × 20 cm^2 area detector with cell (element) size ~3 mm. Corrections were made on a cell-by-cell basis for instrumental backgrounds and detector efficiency (via an ^{55}Fe standard which emits γ-rays isotropically). The data were radially (azimuthally) averaged in the range $0.05 < Q = 4\pi\lambda^{-1} \sin(\theta) < 0.6$ Å^{-1} (where 2θ is the angle of scatter), and were converted to an absolute differential cross section, $d\Sigma/d\Omega(Q)$, by means of pre-calibrated standards.[4c]

Results and Discussion

We begin with a description of the ^{13}C NMR spectra of alkanethiol-stabilized Au cluster compounds dissolved in dilute chloroform solutions. The sections following (SAXS, thermogravimetry, elemental analysis, STM and AFM, DOSY, and DSC) are aimed at defining the composition and dimensions of the clusters, under various circumstances. The number of atoms in the Au core depends on its assumed shape, and models are presented for spherical and cuboctahedral shapes. The concluding sections describe the unusual electronic conductivities of solid films of cluster compounds, including the distance dependence of electron tunneling between the Au cores and the electron exchange dynamics.

NMR Spectra. The experiments seek to understand the behavior of the alkanethiol chains in their unusual environment on the cluster compound surface, as reflected in their NMR spectra. The NMR observations particularly focus on the dependency of resonances on the carbon position relative to the gold−hydrocarbon interface. At this stage of our analysis, the Au core is assumed to have a spherical shape. Figure 1 shows the ^{13}C NMR spectra of alkanethiol-stabilized clusters for three different alkyl chain lengths, octyl (C_8), dodecyl (C_{12}), and hexadecyl (C_{16}). It is readily apparent that the resonances narrow as the carbons are located further from the thiol functionality (see, for example, the decrease in line widths of the ~14 ppm methyl group resonance as the chain length increases). Figure 2 contrasts ^{13}C NMR of the octanethiol monomer with the C_8 cluster, both dissolved in $CDCl_3$. The ^{13}C (and proton, not shown) resonance assignments of the 1-octanethiol monomer (Figure 2a) were based on 2D proton−proton correlation (COSY), 2D heteronuclear proton−carbon correlation (HETCOR), and 2D heteronuclear multiple bond correlation (HMBC) experiments.[6a] The chemical shift assignments for the carbons on the octanethiol chain (Figure 2b) can be reasonably inferred from those of the monomer.

It is apparent from the spectra (Figure 1 and 2) that resonances from carbons closest to the Au core interface—the C_α, C_β, and maybe C_γ—are broadened into the baseline. For example, the C_8 cluster compound (Figure 2b) displays clearly only those carbon resonances that are beyond C_γ, i.e., resonances corresponding to carbons 4 though 8. Moreover, there is a systematic change in the chemical shift and line widths with carbon position relative to the gold−hydrocarbon interface (with respect to the monomer, Figure 2, and Table 1).

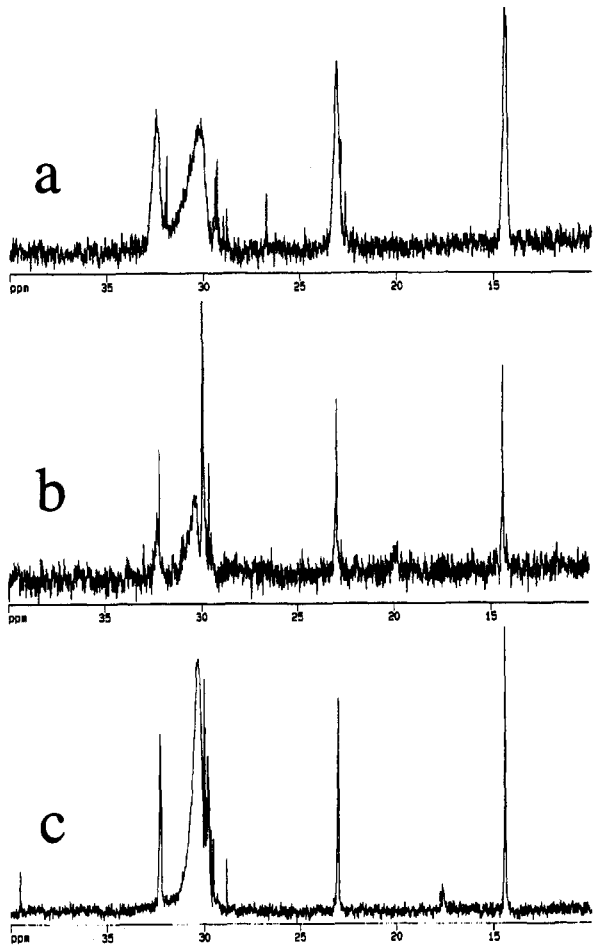

Figure 1. High-resolution ^{13}C NMR spectra of alkanethiol-stabilized Au clusters dissolved in $CDCl_3$: (a) C_8 cluster, (b) C_{12} cluster, and (c) C_{16} cluster.

In the following discussion, these qualitative observations are attributed to the discontinuity in the diamagnetic susceptibility at the gold−hydrocarbon interface and residual dipolar interactions in the alkanethiol monolayer. The spectrum of the C_8 cluster compound will be simulated using calculated magnetic field gradients (chemical shifts relative to the resonances of the monomer) and incompletely averaged C−H bond orientations (a plausible broadening mechanism operative in the hydrocarbon monolayer that stabilizes the nanoparticle).

(6) (a) Croasmun, W. R., Carlson, R. M. K., Eds. *Two-Dimensional NMR Spectroscopy*; VCH; New York, 1994. (b) Glasel, J. A.; Lee, K. H. *J. Am. Chem. Soc.* **1974**, *96*, 970. (c) Lounila, J.; Ala-Korpela, M.; Jokisaari, J.; Savolainen, M. J.; Kesäniemi, Y. A. *Phys. Rev. Lett.* **1994**, *72*, 4049. (d) Flory, P. J. *Macromolecules* **1974**, *7*, 381. (e) Levy, G. C. *Topics in Carbon-13 NMR spectroscopy*; John Wiley and Sons: New York, 1974; Vol. 1. (f) McConnel, J. *The Theory of Nuclear Magnetic Relaxation in Liquids*; Cambridge University Press: Cambridge, 1987. (g) Lee, H. S.; Yang, X. Q.; McBreen, J.; Xu, Z. S.; Skotheim, T. A.; Okamoto, Y. *J. Electrochem. Soc.* **1994**, *141*, 886. (h) Latham, R. J.; Linford, R. G.; Pynenburg, R. A. J.; Schlindwein, W. S.; Farrington, G. C. *J. Chem. Soc., Faraday Trans.* **1993**, *89*, 394. (i) Pace, R. J.; Chan, S. I. *J. Chem. Phys.* **1982**, *76*, 4228. (j) Li, J.; Liang, K. S.; Camillone, N.; Leung, T. Y. B.; Scoles, G. *J. Chem. Phys.* **1995**, *102*, 5012.

(7) Nagahara, L. A.; Hashimoto, K.; Fujishima, A.; Snoden-Ifft, D.; Brice, P. B. *J. Vac. Sci. Technol. B* **1994**, *12*, 1694.

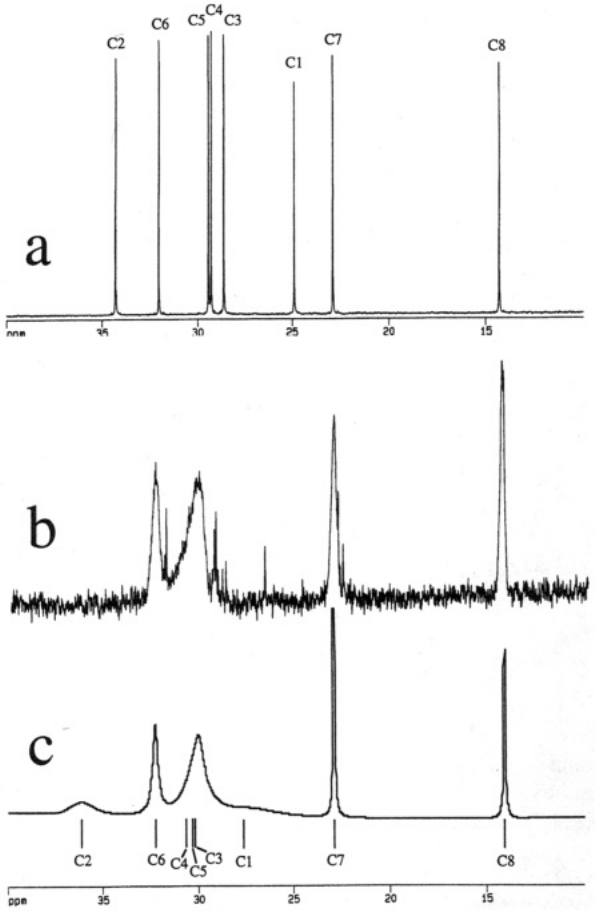

Figure 2. High-resolution ^{13}C NMR spectra of (a) 1-octanethiol, (b) 1-octanethiol-stabilized gold cluster compound dissolved in $CDCl_3$, and (c) calculated spectrum.

Table 1. 1-Octanethiol-Stabilized Gold Clusters: ^{13}C Chemical Shifts δ_i (in Frequency Relative to Octanethiol Monomer), and Average Carbon Distances $\langle x_i \rangle$ (from the Gold−Hydrocarbon Interface)

carbon i	$\langle x_i \rangle_{b=90°}$/Å	$\langle x_i \rangle_{b=22°}$/Å	$\delta^{obs}{}_i$/Hz	$\delta^{calc}{}_i$/Hz[a]
1	1.40	1.40		190
2	2.79	2.79		145
3	4.01	4.15		116
4	4.80	5.14	109	95
5	5.66	6.50	55	60
6	6.32	7.35	29	31
7	6.94	8.58	14	24
8	7.47	9.30	5	15

[a] Taking $b = 22°$.

The distribution of the magnetic field intensity H for a sphere of radius R_{CORE} in a uniform external field H_0 can be expressed as[6b,c]

$$H(R>R_{CORE}) = \left[1 + \frac{2(\mu - \mu_{CORE})}{2\mu + \mu_{CORE}} \frac{R^3_{CORE}}{R^3} P_2(\cos\theta)\right] H_0 \mathbf{e}_{||} + \left[\frac{3(\mu - \mu_{CORE})}{2(2\mu_{CORE} + \mu)} \frac{R^3_{CORE}}{R^3} \sin 2\theta\right] H_0 \mathbf{e}_{\perp} \quad (1)$$

where μ_{CORE} and μ are respectively the magnetic permeabilities of the gold (sphere) and the (hydrocarbon) surrounding medium ($\mu = 1 + 4\pi\chi$, where χ is the susceptibility); θ is the angle between the position vector $\mathbf{R}$ and $\mathbf{e}_{||}$, the unit vector in the direction of the uniform field $\boldsymbol{H}_0$ of the NMR spectrometer (Figure 3, roughly to scale), and $P_2(\cos\theta) = (3\cos^2\theta - 1)/2$.

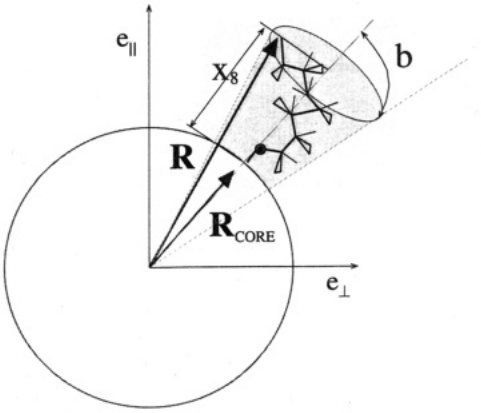

Figure 3. A schematic diagram of a 1-octanethiol-stabilized gold cluster indicating the radius of the gold nanoparticle R_{CORE}, the radial distance R, and the average normal distance $\langle x_8 \rangle$ of carbon 8 from the center of the Au core and the gold−hydrocarbon interface, respectively; b is the half-angle of the conical packing constraint.

According to eq 1 the average (θ-independent) magnetic field[6e] $\langle H_i \rangle$ at the ith carbon (C_i) is a function of the susceptibilities, the radius of the Au core, R_{CORE}, and the (average) distance of C_i from the center of the Au cluster:

$$\langle H_i \rangle = \left[\frac{2a+1}{2} - \frac{a-1}{\sqrt{-3a(a+2)}} \arcsin\left(\frac{\sqrt{-3a(a+2)}}{1-a}\right)\right] H_0 \quad (2)$$

where

$$a = \frac{\mu - \mu_{CORE}}{2\mu_{CORE} + \mu} \frac{R^3_{CORE}}{R_i{}^3}$$

The radial distance, R_i, was estimated based on the standard alkane rotational isomeric state[6d] (RIS) chain statistics in conjunction with a steric constraint on the space sampled by an alkyl chain covalently attached to an impenetrable (gold) interface. In the case of the C_8 monolayer, a lateral constraint is placed on the RIS average, one originating from packing or excluded-volume interactions among the close-packed alkanethiols on the nanoparticle's surface. It is simply introduced in the form of a conical cutoff (adjusted via the half-angle b, see Figure 3) such that conformations of the chain which penetrate this constraint surface are rejected from the RIS average, over all conformations of the pendant C_8 chain. The single adjustable parameter b is obtained by comparisons between the calculated and experimental relative chemical shifts and line widths. The corresponding excluded surface area per chain for the optimum b value, 0.185 nm^2 or *ca.* 98 chains on a sphere of radius R_{CORE} = 12 Å, is consistent with surface number densities of alkanethiol (90 and 126 chains) deduced from other measurements and models (*vide infra*). The RIS average yields the average normal distance $\langle x_i \rangle$ of the ith carbon from the gold−hydrocarbon interface; $R_i = R_{CORE} + \langle x_i \rangle$ is required for the computation of $\langle H_i \rangle$ in eq 2.

Table 1 shows the calculated values of $\langle x_i \rangle_b$ for an unconstrained alkanethiolate chain ($b = 90°$) and for one with a conical cutoff value ($b = 22°$). The relation between the frequency and the magnetic field is obtained from $h\nu = \gamma_N \beta_N \langle H_i \rangle$ where γ_N is the gyromagnetic ratio and β_N is the nuclear Bohr magneton. The observed ($\delta^{obs}{}_i$) and calculated chemical shifts ($\delta^{calc}{}_i$) are given in columns four and five respectively of Table 1. The $\delta^{calc}{}_i$ for carbons on the octanethiol chains of the C_8 cluster are computed using the RIS values for $\langle x_i \rangle$ with R_{CORE}

Table 2. 1-Octanethiol−Stabilized Gold Clusters: ^{13}C Line Widths $1/\pi T_2$ and Average C−H Order Parameters $\langle P_2(\cos\alpha_i)\rangle$ (Relative to the C−H Bond of C_1)

carbon i	$\langle P_2(\cos\alpha_i)\rangle_{b=90°}$	$\langle P_2(\cos\alpha_i)\rangle_{b=22°}$	$(1/\pi T_2)^{obs}$/Hz	$(1/\pi T_2)^{calc}$/Hz
1	1.00	1.00		
	114			
2	0.43	0.71		
	58			
3	0.11	0.71		
	58			
4	0.03	0.57	42	37
5	0.00	0.42	21	20
6	0.01	0.30	15	12
7	0.00	0.15	10	3
8	0.01	0.09	8	1

= 12 Å (the SAXS core size results for the C_{12} cluster, *vide infra*) to obtain $\langle H_i\rangle$.

Next we consider the origins of the position-dependent broadening of the resonances of the C_8 chain (Table 2). Since the calculated $\delta^{calc}{}_i$ depend on $\langle x_i\rangle$ and R_{CORE}, the position-dependent line widths could be caused by a distribution of R_{CORE} values. While there is some intimation of size dispersity in the hydrodynamic radii of the overall cluster compound (see DOSY section), the SAXS data suggest a narrow distribution of Au *core* radii. Assuming then that R_{CORE} is indeed narrowly distributed, another mechanism is needed to explain the observed position-dependent broadening of the carbon resonances. Some possibilities[6e,f] include the spin−lattice relaxation rate $(1/T_2)$ dependence on the magnetic field anisotropy (due to θ dependence in eq 1 in the long correlation time τ_c limit for nanoparticle reorientation), the chemical shift anisotropy, and the residual heteronuclear (C−H) dipolar interactions. From qualitative estimates of each, we conclude that only the latter factor is of sufficient magnitude to explain the observed broadening, assuming a monodisperse R_{CORE}.

The dipolar interaction mechanism contributes to the broadening as follows: The line width $(1/\pi T_2)$ can be approximated by[6e]

$$\frac{1}{\pi T_2} = \frac{1}{20\pi}\left[\frac{g_C{}^2 g_H{}^2 \beta_N{}^4}{h^2 R^6}\right][\langle P_2(\cos\alpha_i)\rangle]^2[4\tau_C^+ + f(\omega_H - \omega_C) + 3f(\omega_C) + 6f(\omega_H) + 6f(\omega_H + \omega_C)]$$

$$f(\omega_i) = \frac{1}{1 + \omega_i{}^2\tau_i{}^2}$$

$$\tau_C = \frac{4\pi[R_{CORE} + R_{CHAIN}]^3\eta}{3k_BT} \qquad (3)$$

ω_C and ω_H are the Larmor frequencies ($\omega_H = 4\omega_C$, $\omega_C \sim 75$ MHz) corresponding to the applied magnetic field H_0 and R_{CHAIN} is the increment to cluster radius associated with the alkanethiol chain. A single correlation time τ_C is used to account for the reorientation of the C−H bond vectors in the following way. The overall cluster reorientational diffusion time ($\tau_C = 6.5 \times 10^{-9}$ s) is derived from the Debye relation using a sphere hydrodynamic radius $R_{HYDRODYNAMIC} = R_{CORE} + R_{CHAIN}$ and $\eta = 0.58$ cP for chloroform at 300 K. R_{CHAIN} is assumed to equal $\langle x_8\rangle$, the average radial distance of the methyl from the C_8 cluster gold surface. In this single-correlation-time model, the intraparticle dynamics—rapid reorientation of the C−H bond vectors as the alkyl chain samples accessible conformations—is accounted for with the factor $[\langle P_2(\cos\alpha_i)\rangle]^2$. This factor accounts for "pre-averaging" the ith C−H dipolar interaction; similar modeling of NMR interactions has been employed for model membranes.[6i] In the RIS approximation, $P_2(\cos\alpha_i)$, where α_i is the angle between the C−H bond on C_i and the static (relative to the Au core) C−H bond on carbon 1, was computed for each carbon with the RIS method using the conical constraint (Table 2). There is reasonable qualitative agreement between the observed and calculated line widths using this approximate model (Table 2). Figure 2c shows the simulated ^{13}C spectrum for the C_8 cluster compound using the data in Tables 1 and 2 to derive the spectrum. According to the simulation the carbon 3 resonance is shifted relative to that in the monomer and lies in the envelope comprised of resonances associated with carbons 4 and 5; on the other hand, according to this ideal model it is not obvious why the carbon 2 resonance is not observed. More refined simulations including nonspherical nanoparticles and a distribution of R_{CORE} values are under way to better understand these spectra.

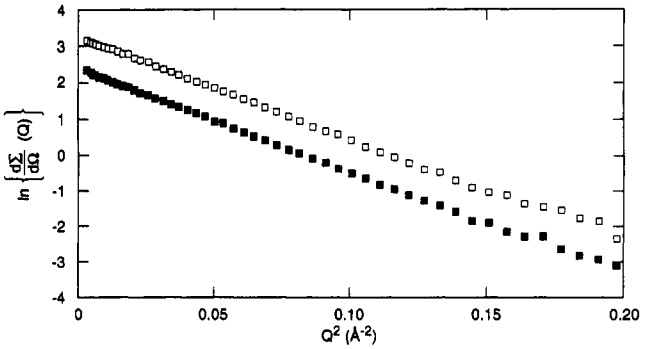

Figure 4. Guinier plot of small-angle X-ray scattering of a solution of the C_{12} cluster dissolved in hexane.

The idealized modeling assumes that the isomerization of the alkyl chains of the clusters is rapid on the NMR time scale. Tables 1 and 2 include the calculations of radial distance $\langle x_i\rangle$ and C−H "order parameters" $\langle P_2(\cos\alpha_i)\rangle$ for carbons in an *isolated* octanethiol unit covalently attached to a flat ($b = 90°$) Au surface, i.e., without the conical constraint. When these values are compared to the RIS averages computed *with* a conical constraint (with optimized half-angle $b = 22°$), one can gauge the magnitude of the packing constraints present within the monolayer. The calculations suggest that for carbons 2 and 3, the constrained isomerization of the chains has marginal influence on the mean *distance* of these carbons from the gold surface (Table 1); however, there is a measurable influence on the *orientational freedom* of carbons 2 and 3 (Table 2). The latter influence persists throughout the entire chain and indicates that the packing constraint induces about a 20% increase in the average distance between the Au core and the terminal methyl group. Hence we conclude that the nature of the methylene alkyl chains on the octanethiol-stabilized Au clusters is measurably different from free chains. At the same time, it would appear that in these monolayers, with high curvature of the underlying surface, there is considerable intrachain mobility relative to the well-ordered chains comprising self-assembled monolayers on flat gold surfaces.[1,6j]

SAXS Measurements. Figure 4 shows a Guinier plot [log $d\Sigma/d\Omega$ *vs* Q^2], for two different concentrations of the C_{12} cluster in hexane (7.8 and 3.8 g/100 cm^3). The plots are remarkably linear up to $Q \sim 0.4$ Å^{-1} and the slope gives the radius of gyration (R_G) (i.e., the root-mean-square distance of all scattering elements from the center of gravity). The Guinier approximation is based on the assumption[4d] of dilute non-interacting particles with $d\Sigma/d\Omega(Q) \sim d\Sigma/d\Omega(0)\exp(-Q^2R_G2/3)$. The slope is the same for both samples, meaning that R_G is independent of the concentration and $d\Sigma/d\Omega(0)$ is proportional to concentration, indicating that the assumptions are reasonable.

A further assumption of the Guinier analysis is that $Q^2R_G^2/3 \ll 1$, a condition easily fulfilled for the minimum Q value (0.05 $Å^{-1}$), since R_G is *ca.* 9.2 Å for both concentrations, giving $Q_{MIN}^2R_G^2/3 \sim 0.07$. As $Q_{MAX}2R_G2$ is increased, the measured R_G is virtually independent of the limiting value. For example, for the 3.8 wt % sample, values of 9.25, 9.23, 9.27, and 9.24 Å are derived from the fitting as $Q_{MAX}^2R_G^2/3$ is progressively increased from 0.45 to 0.52, 0.60, 0.66, and 0.96. Thus no systematic trend is evident, so a mean $R_G = 9.24 \pm 0.05$ Å was averaged over the various Q ranges and concentrations.

For homogeneous non-interacting particles, suspended in dilute solution, the SAXS cross section is given by

$$\frac{d\sum(Q)}{d\Omega} = (\varrho_{ep} - \varrho_{es})^2 r_T^2 N_p V_p^2 P(Q) \qquad (4)$$

where ρ_{ep} and ρ_{es} are the electron densities of the particle and solvent respectively, $r_T = 0.282 \times 10^{-12}$ cm is the (Thompson) scattering length of an electron, N_p is the number of particles per unit volume, V_p is the volume, and $P(Q)$ is the particle form factor. At zero Q, $P(0) = 1$, so the extrapolated cross section $d\sum/d\Omega(0)$ can be calculated from eq 1 and compared to the experimentally measured values.

The contribution of the cluster compound components to the SAXS intensity is weighted by the scattering contrast with the solvent.[4e] The gold core has a very high electron density compared to the hexane value (0.24 $e^-/Å^3$), which is virtually the same as the alkanethiol, so the scattering is dominated by the gold−solvent contrast. This supports another assumption of the Guinier model, as the volume fraction of the Au core is <1% for both concentrations, which is consistent with the dilute solution hypothesis.

Taking the Au content of the cluster as 76% (see TGA and Elemental Analysis below), and that the particle is spherical, we can estimate[4e] the radius $R_{CORE} = (5/3)^{0.5}R_G = 11.93 \pm 0.06$ Å, with a volume of 7110 ± 110 $Å^3$. Assuming that the particles contain 400 atoms leads to a core density of 18.4 gm/cm^3 and estimates of the ($Q = 0$) extrapolated cross section [$d\sum/d\Omega$ (0)] of 42.6 cm^{-1} (7.8 gm Au/100 cm^3), and 20.9 cm^{-1} (3.8 gm Au/100 cm^3). These estimates are much larger than the experimentally observed cross sections (26.6 and 11.2 cm^{-1}, respectively). Assuming 300 atoms in the core leads to a density of 13.8 gm/cm^3 and theoretical cross section estimates of 30.8 and 15.9 cm^{-1}, which are much closer to the measured values. The overall error is ±15%, due to uncertainties in the absolute calibration and concentration.

The use of absolute units (cm^{-1}) is not essential for the measurement of spatial dimensions (e.g. R_G). However, because the cross section varies as the sixth power of the dimensions,[3d] it is a very sensitive indicator of whether an appropriate structural model has been chosen and comparison of the measured and calculated cross sections favors a smaller number of atoms (~300) in the core.

Thermogravimetry. In all cases, the mass losses exhibited by the cluster compounds were single, well-defined steps of *ca.* 100 °C width beginning at 230, 266, and 310 °C for the C_8, C_{12}, and C_{16} clusters, respectively. The residue was a coarse golden powder. The mass losses were 19.74% (C_8), 24.07% (C_{12}), and 33.54% (C_{16}) which correspond to quantitative loss of the alkanethiolate chains. The temperature dependence of the mass losses indicates that the thermal stability of the alkanethiol-stabilized Au cluster compounds increases with increasing chain length.

Elemental CHS Analysis. Compositional analysis for C, H, S, and Au performed commercially appeared to under-report the Au content; results for the latter appear to be flawed. Analyses for the C_8 and C_{12} clusters (see Experimental Section) did not sum (C + H + S + Au) to 100%: the sums are C_8 95.46%, C_{12} 94.47%, and C_{16} 99.81%. On the other hand, mass loss in the TGA and percent (C + H + S) from the elemental analysis were in better agreement: C_8 elemental 20.67%, TGA 19.74%; C_{12} elemental 25.69%, TGA 24.07%; C_{16} elemental 35.47%, TGA 33.54%. Also, the fractional amounts of C, H, and S (i.e., C/C + H + S, etc.) found in the elemental analyses were all in close agreement with the composition of the C_8, C_{12}, and C_{16} alkanethiol monomers; the combined absolute errors ($|\Delta\%C_{theo\text{-}expmt}| + |\Delta\%H_{theo\text{-}expmt}| + |\Delta\%S_{theo\text{-}expmt}|$) were C_8 0.70%, C_{12} 1.28%, and C_{16} 0.43%. The weight fraction of C + H + S is used below in modeling of the cluster dimensions.

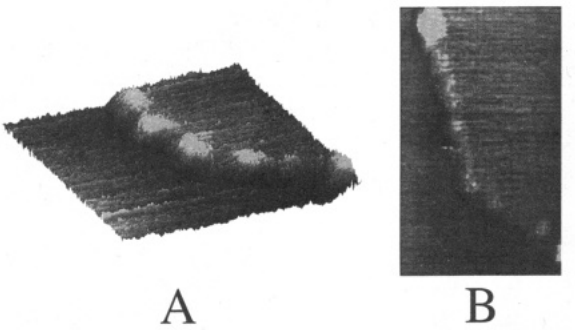

Figure 5. STM images of individual C_{12} cluster molecules on HOPG. (panel A) 20 × 20 nm surface plot with 30° pitch angle; (panel B) 18 × 30 nm gray scale image. The bias voltage and tunneling current are 500 mV and 0.5 nA, respectively.

STM and AFM Measurements of Cluster Sizes. Figure 5 is a typical image obtained on an HOPG surface on which a dilute C_{12} cluster solution had been evaporated. Initial STM scans are noisy and exhibit no clear images, but after a few scans the image clears and the cluster compound appears as spherical protrusions lying along HOPG lattice step edges. HOPG step edges are normally quite sharp and the protrusions seen in Figure 5 are atypical of artifactual images previously seen on HOPG or of images that we have ourselves previously seen on HOPG, so the protrusions are believed to represent individual cluster molecules. Line scans indicate that the imaged clusters lie predominantly at double-atomic step edges. Clusters were not observed on smooth HOPG terraces, suggesting that the alkanethiol clusters do not adsorb strongly on HOPG and are pushed aside by the scanning tip, but do become lodged at step edges. Recording the apparent size of 120 cluster molecules (measured edge-to-edge) for each of the three alkanethiol preparations indicates no significant difference in dimension between C_8, C_{12}, and C_{16} clusters. The most populated cluster diameter falls in the regime of 3.9 to 4.5 nm and the percentages of C_8, C_{12}, and C_{16} clusters that fall within this regime are 52, 48, and 62%, respectively.

A recent report[8] comparing STM and TEM measurements of tetraalkylammonium-stabilized palladium clusters concluded that TEM images only the core whereas STM images the total (organic + core) diameter. Our STM images show a larger radius (21 ± 1.5 Å) than TEM[2] (10−13 Å) or SAXS (11.9 Å, vide supra, which also images the Au core), and thus may reflect the overall cluster dimension. Convolution of the particle size with the STM tip dimension may cause the STM images to overestimate the true cluster size. Nonetheless, the STM size estimates agree fairly closely with the DOSY hydrodynamic radii (vide supra) and are within experimental uncertainty of

(8) Reetz, M. T.; Helbig, H.; Quaiser, S. A.; Stimming, U.; Bruer, N.; Vogel, R. *Science* **1995**, *267*, 367.

Table 3. Cluster Compound Radii, Å

	Au core radii		scanning microscopy		cluster radii	
alkanethiol cluster	SAXS	TEM[a]	AFM[b]	STM[c]	DOSY[d]	solid state core spacing[e] (density)
C8				21 ± 1.5	15	18.4 ± 0.8
C12	11.93 ± 0.05	10−13	11 ± 5	21 ± 1.5	22	19.3 ± 0.3
C16				21 ± 1.5	24	21.0 ± 0.7

[a] Brust el.[2a] found a broad size distribution, and cuboctahedral and icosahedral shapes, presumably imaging the gold core. [b] Tapping-mode AFM measurement, one-half of height in line scan. [c] STM radii are one-half the edge to edge dimensions in Figure 5, uncorrected for tip convolution. [d] Results for diffusion coefficients of the three clusters were $D = 2.6(\sigma \pm 0.3) \times 10^{-6}$, $2.3(\sigma \pm 0.2) \times 10^{-6}$, and $1.6(\sigma \pm 0.2) \times 10^{-6}$ cm²/s, in $CDCl_3$, CD_2Cl_2, and $CDCl_3$, for C_8, C_{12}, and C_{16}, respectively.

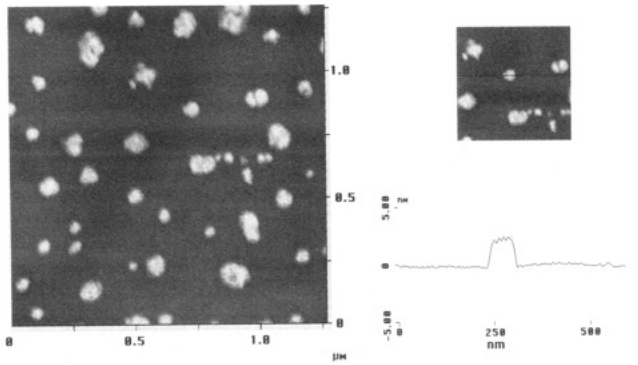

Figure 6. Tapping-mode AFM image of C_{12} cluster aggregates adsorbed on etched mica.

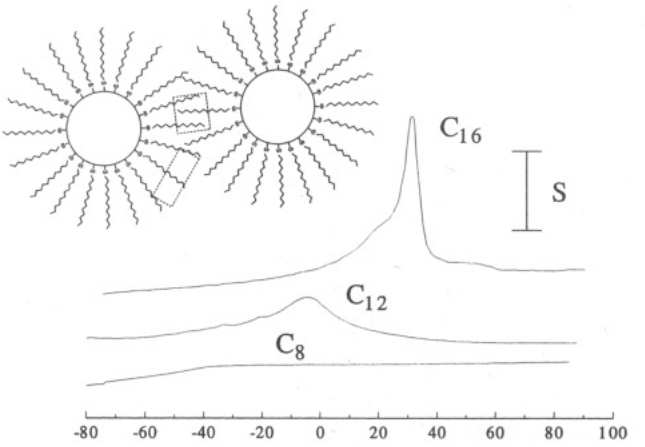

Figure 7. Differential scanning calorimetry of the solid, dry C_8, C_{12}, and C_{16} clusters. $S = 100$ (C_{16} and C_8) and 33 μW/mg (C_{12}). Inset is a to-scale cartoon of C_{12} clusters in which possible regions of crystallinity are indicated, through chain interdigitation (square box) or intersticial folding (rectangular box).

cluster radii measured from densities of solid cluster samples (vide infra). Given the available chain mobility indicated by the NMR analysis, however, it is important to note that the *apparent* overall cluster radius may reflect its *environment* (e.g., lying on a surface in air *vs* dissolved *vs* solid state).

Height measurements by tapping-mode AFM indicate a slightly smaller particle. Figure 6 shows images on a flat mica terrace which appear to be C_{12} cluster aggregates. In general, the aggregates are much broader than they are high, and no significant difference in height between large and small aggregates was detected, indicating that the groups consist of a single layer of cluster particles. The average height of such aggregates was 2.2 ± 0.9 nm, very nearly double the SAXS radius of the gold cores.

DOSY Hydrodynamic Radii and Distributions. The hydrodynamic radii of alkanethiol-stabilized Au clusters dissolved in $CDCl_3$ and CD_2Cl_2 were determined using diffusion-ordered ^{1}H NMR spectroscopy (DOSY). The distributions of diffusion coefficients, $G(D)$, of the clusters were determined by fitting the NMR methylene peak areas (A) versus q^2 to the following equation by means of the program CONTIN:[5d,e]

$$A = \int A_0 G(D) \exp[-Dq^2(\Delta - \delta/3)]\, dD \qquad (5)$$

where A_0 is the methylene peak area when gradient pulse area is $q = 0$ (taking relaxation into account), Δ is the diffusion time, and δ is the duration of the gradient pulses. The distribution function $G(D)$ determined by this method is weighted by the number of protons on each diffusing cluster particle. The effective hydrodynamic radii R_H were calculated from measured average D values with the Stokes−Einstein equation:

$$R_H = \frac{k_B T}{6\pi\eta D} \qquad (6)$$

where k_B is the Boltzmann constant, T absolute temperature, and η the solvent viscosity. The viscosities of CD_2Cl_2 and $CDCl_3$ not being available, those of CH_2Cl_2 ($\eta = 0.43$ cP) and $CHCl_3$ ($\eta = 0.56$ cP) at 295 K were employed. Average diffusion coefficients, standard deviations, and computed Stokes−Einstein radii are listed in Table 3. The width of the distribution function (20−30% returned by CONTIN) suggests some polydispersity in the hydrodynamic radii. If the gold cores are in fact monodisperse as indicated by the SAXS results and Figure 4, this raises as yet unresolved questions about uniformity in the number or steric features of alkanethiolate chains attached to the Au cores.

Differential Scanning Calorimetry. Figure 7 shows differential scanning calorimetric (DSC) heating curves obtained for dry samples of the three alkanethiol-stabilized cluster compounds, from −100 to +100 °C. Multiple C_8 cluster experiments revealed no discernable transition, while the C_{12} and C_{16} clusters exhibit broad endotherms corresponding to 7.7 ± 3 ($n = 3$) J/g (C_{12}) and 18 ± 1 ($n = 2$) J/g (C_{16}). Assigning this heat to the alkanethiol mass fraction in the cluster (based on the TGA analysis) gives transition enthalpies of 6.5 kJ/mol for dodecanethiolate and 14 kJ/mol for hexadecanethiolate monolayers. The melting heats for pure dodecane and hexadecane are smaller (37 and 50 kJ/mol, respectively), so that these melting transitions involve a portion, not all, of the hydrocarbon chains.

The ordered portion of the alkanethiol chains could be (i) that nearest the Au core, or (ii) that lying astride a normal drawn between adjacent Au cores (square box, Figure 7 inset), or (iii) that lying in the interstices of the packing of the clusters (rectangular box, inset). The first possibility is unlikely given the absence of a thermal feature for the C_8 cluster. As for possibilities (ii) and (iii), the small surface curvature radius of the Au core surface means that, even with close-packed Au−S

(9) Watanabe, J.; Ono, H.; Uematsu, I.; Abe, A. *Macromolecules* **1985**, 2141.

chemisorption sites, the alkanethiol chain *termini* must be much less closely packed than the C_α carbons. For the C_{12} cluster, for example, the terminal methyl group density (per unit area of outer particle surface) would be only *ca.* 18% that of the density of anchor points at the Au−thiol interface if the all-trans chains extend radially. This change in chain density would be greater (~13%) and less (~27%) for C_{16} and C_8 clusters. This packing change would readily permit interdigitation of the chains of adjacent cluster molecules (Figure 7, cartoon inset, box), and the thermal features of Figure 7 may then represent melting of interdigitated regions. Such a picture is appealing by analogy to that described by Watanabe *et al.*[9] from DSC observations of "hairy rod" polymers (rigid α-helical rods with alkyl side chains) bearing differing side chain lengths. Watanabe et al. concluded that this type of melting transition has a heat of approximately 4.0 kJ/mol of interdigitated CH_2 groups. Applying this analysis to our data implies, approximately, an average of 2 interdigitated and ordered CH_2 groups per chain for the C_{12} cluster and 3−4 interdigitated CH_2 groups per chain of the C_{16} cluster, i.e., ordered chain interdigitation begins *ca.* 10−12 units from the Au core. Given that all chains on adjacent spheres cannot (for geometrical reasons) equally interdigitate, the longest segments of ordered chain interdigitation probably exceed the above numbers; this in fact is consistent with density measurements on solid clusters (*vide infra*). The possibility of interdigitation is important in electronic conductivity measurements since it affects the Au core-to-core distance.

Cluster Dimensions and Molecular Weight. Model of the Cluster Core. The following enlarges on a dimensional model of the cluster molecules and their cores.

From the present data, estimates of the molecular weight and thiolate surface coverage of the cluster require structural models of the gold core *shape*. Such models reflect the numbers of gold atoms on the surface and in the entire particle, for comparison to elemental analysis results. Two shapes are modeled, a sphere and a cuboctahedron.

The spherical model takes the gold core as a sphere with density ρ_{Au} (assuming that of bulk gold) covered with a "skin" of hexagonally close-packed gold atoms. We label this a "continuum" model. The radius of the "skin" is taken as the center of the atoms on the skin (at $R_{CORE} - R_{Au}$), to avoid overestimating the number of surface atoms. The relation is

$$\chi_{organic} = \frac{4\pi(R_{CORE} - R_{Au})^2(\varrho_{HCP})(MW_{thiol})\gamma}{4\pi(R_{CORE} - R_{Au})^2(\varrho_{HCP})(MW_{thiol})\gamma + {}^4/_3\pi R^3_{CORE}(\varrho_{Au})(AW_{Au})} \quad (7)$$

where $\chi_{organic}$ is the mass fraction of alkanethiolate in the cluster, R_{Au} the crystallographic radius of a gold atom (0.145 nm),[10a] ρ_{HCP} the number density of surface gold atoms (13.89 atoms/nm^2, assuming hexagonal close packing), MW_{thiol} the alkanethiol molecular weight in mass/molecule, γ the coverage (ratio of alkanethiolates to surface Au atoms),[1i,j] ρ_{Au} the atom density of bulk gold (58.01 atoms/nm^3), and AW_{Au} the Au atomic weight in mass/atom. The numerator in eq 7 and the first term in the denominator represent the alkanethiolate mass on the surface of the Au core. The second term in the denominator represents the Au core mass. Since $\chi_{organic}$ depends on the model's prediction of the surface:volume ratio of gold atoms, we checked it with a simple computer program. Assuming a "spherical" core, the program counts the number of surface and total atoms contained within spheres of various radii superimposed on an FCC lattice.[10b] The FCC and "continuum" predictions of surface:volume atom ratios were in good agreement in the expected sphere size range.

The C_{12} surface coverage of alkanethiolates was determined as $\gamma = 0.66$ by solving eq 7 taking the R_{CORE} value determined by SAXS (11.9 Å) and $\chi_{organic}$ from the elemental and TGA analyses. The spherical model, for this R_{CORE} value, predicts that the core will contain 409 Au atoms, of which 191 lie on its surface. Thus, if this model is accurate, there are 126 alkanethiolate chains or 2 for every 3 surface gold atoms. This coverage is *twice* that seen for monolayers[1i,j] on planar hexagonally close-packed Au(111) surfaces ($\gamma = 0.33$), requiring Au−S sites to be more densely packed on the surface of the Au cluster compound. This may reflect the small R_{CORE} value which splays the attached alkanethiol chains outward from one another, relieving steric crowding, and/or the reactivity of atoms on the highly curved core surface (relative to planar gold).

Turning to the other core model, high-resolution TEM[2a] of the C_{12} cluster suggested cuboctahedrally-shaped cores, so we consider a cuboctahedron for the C_{12} clusters. A perfect cuboctahedral gold cluster closest to a 12 Å "radius" consists of either 309 or 561 total atoms[3a,11] (so-called "magic numbers"), and has 162 or 252 surface atoms, respectively. Modeling the clusters as Au_{309} and Au_{561} cuboctahedra returns γ values of 0.59 and 0.69, respectively, which are not very different from those predicted for "spherical" cores. This is because cuboctahedra have nearly the same ratio of surface atoms to total atoms as do the fictitious spheres of the "continuum" model, eq 7. Taking the cuboctahedron structure into account adds to this picture, moreover. A Au_{309} cluster would have 60 "edge" surface atoms, and 102 on flat faces, an arrangement leaving precisely one alkanethiolate per 3 gold atoms on the flat faces (in agreement with the $\gamma = 0.33$ observed for alkanethiolate monolayers on hexagonally close-packed planar gold[1i,j]) if all "edge" atoms are assumed to bind one (sterically relatively unencumbered) alkanethiolate.

We do not have in hand SAXS determinations of the core radii of the C_8 and C_{16} clusters, but returning to the spherical model, the "continuum" model eq 7 can be solved for R_{CORE} assuming the coverage result from the C_{12} cluster ($\gamma = 0.66$). This gives $R_{CORE} = 10.7$ Å (C_8 clusters) and 8.5 Å (C_{16} clusters, Table 3). Considering the approximations, there clearly is not a *large* change in the average core size with alkanethiol chain length. Further SAXS measurements will resolve these features.

Last, analysis of the SAXS intensities in the C_{12} cluster R_{CORE} measurement suggests a Au core population close to that of the cuboctahedral model. Equation 7 with $R_{CORE} = 11.9$ Å (the SAXS result) and $\gamma = 0.66$ predicts an average C_{12} cluster "molecular weight" of 106 000 g/mol, in the mass range of many biomolecules. The 309 and 561 atom cuboctahedra MW would be 80 000 and 140 000 g/mol, respectively. Mass spectral molecular weight measurements should help to resolve the shape issue, and this measurement will be part of future efforts.

Density and Au Core Spacing in Solid Cluster. The core−core spacing in solvent-free cluster is important in analysis of cluster compound electronic conductivity, and provides a point of comparison to the Au core and hydrodynamic radii measurements. From the cluster densities, mass fraction of gold (TGA analysis), and the gold core mass (M_{CORE}, 1.21×10^{-19} g based on SAXS radius and eq 7 and assuming a simple cubic packing and that R_{CORE} is the same for all the clusters), the concentrations (C_{CORE}) of cluster particles in the solid state and their center−

(10) (a) Kittel, C. *Introduction to Solid State Physics*, 6th ed., Wiley: New York, 1986. (b) Inoue, H.; Ichiroku, N.; Torimoto, T.; Sakata, T.; Mori, H.; Yoneyama, H. *Langmuir* **1994**, *10*, 4517.

(11) (a) Schon G.; Simon, U. *Colloid Polym. Sci.* **1995**, *273*, 101. (b) Schon G.; Simon, U.; *Colloid Polym. Sci.* **1995**, *273*, 202.

Table 4. Densities and Concentrations of Solvent-Free Cluster Compounds

alkanethiol	cluster density, g/cm^3	Au core concn, M	center−center[a] Au core spacing, Å	edge−edge[b] Au core spacing, Å
C_8	3.32 ± 0.24 ($n = 3$)	0.033	36.9 ± 0.8	13.1 ± 0.8
C_{12}	3.06 ± 0.07 ($n = 2$)	0.029	38.6 ± 0.3	14.8 ± 0.3
C_{16}	2.70 ± 0.15 ($n = 3$)	0.022	42.1 ± 0.7	18.3 ± 0.7

[a] One-half of these values is the effective cluster radius in the solid material, Table 3. [b] Center-to-center core spacing minus twice R_{CORE} where $R_{CORE} = 11.9$ Å.

Table 5. Electronic Properties and Proposed Electron Hopping Rate Constants through Cluster Solids

alkenethiol	room temp (30 °c)[a] conductivity, ω^{-1} cm^{-1}	Arrhenius intercept[b] $\sigma_0 e^{-\delta\beta}$, Ω^{-1} cm^{-1}	Arrhenius[b] E_{ACT}, kj/mol	first-order rate constant[c] $\rho k_{ex} C_{\pm}$, s^{-1}	bimolecular rate constant[d] ρk_{EX}, M^{-1} s^{-1}	high-field parameter ρ	av % dev of fit
C_8	$1.8 \pm 0.8 \times 10^{-5}$ ($n = 3$)	$5.4 \pm 1.1 \times 10^{-4}$ ($n = 2$)	9.6 ± 0.6	$6.5(\pm 2.9) \times 10^6$	2×10^{10}	2.2 ± 0.2 ($n = 7$)	6
C_{12}	$2.3 \pm 0.8 \times 10^{-7}$ ($n = 10$)	$7.3 \pm 3.0 \times 10^{-5}$ ($n = 4$)	16 ± 3	$8.6(\pm 2.8) \times 10^4$	7×10^8	2.5 ± 0.5 ($n = 11$)	6.6
C_{16}	$2.8 \pm 1.1 \times 10^{-9}$ ($n = 7$)	$1.1 \pm 0.7 \times 10^{-6}$ ($n = 4$)	19 ± 2	$1.2(\pm 0.5) \times 10^2$	2×10^8	2.6 ± 0.1($n = 7$)	6.7

[a] From small-amplitude potential sweeps. [b] Figure 8, left side. [c] From high-field fit of eq 11 or from small-amplitude conductivities, at room temperature. [d] Using the approximate model eq 11 and the average Arrhenius-derived activation energies to calculate the carrier concentrations, $C_{\pm}$.

center spacings (δ_{CORE}) are

$$C_{CORE} = \varrho_{COLLOID}(1 - \chi_{ORGANIC})\frac{N_A}{M_{CORE}}$$

$$\delta_{CORE} = \frac{1}{\sqrt[3]{C_{CORE}}} \qquad (8)$$

These results (Table 4) show that dry cluster compound densities decrease with increasing alkanethiolate length, and corresponding center-to-center spacings (δ_{CORE}) increase. An important result is that the corresponding edge−edge core spacings *are considerably shorter than twice the length of the alkanethiolate chains* and are actually closer to a single *all-trans* chain length, 11.2, 16.2, and 21.1 Å for C_8, C_{12}, and C_{16} chains, respectively. Chain interdigitation and/or folding (at least in the solid phase) is suggested by this result (cartoon, Figure 7).

Summary of Cluster Size Measurements. Table 3 summarizes size data and group measurements according to sensitivity to Au core size (left) and to overall cluster size (right). The SAXS and TEM C_{12} cluster measurements should reflect only core size and are consistent with one another.

In Table 3, right side, the DOSY and solid state (density) core spacing data reflect overall cluster size in solution and solid state, respectively. The hydrodynamic radius R_H for the C_8 cluster (15 Å) is somewhat less than the sum, 19.8 Å, of the Au core radius (10.5 Å, inferred from elemental analysis data, *vide supra*) and the average chain extension inferred from analysis of the NMR data (9.3 Å, Table 1). The R_H results are reasonably close to the density-derived cluster radii but vary more with alkanethiol chain length; this may simply reflect a difference between average chain conformations in dissolved clusters (the chain termini being well solvated) *vs* solid state clusters (the chain termini being strongly interdigitated and/or folded).

It was not at the outset obvious whether STM and AFM would respond more sensitively to the Au core or overall cluster size. The STM results are reasonably close to the DOSY and density results, strongly implying that the STM tip does not thrust through the alkanethiol monolayer but responds to the monolayer skin as well as the Au core. This is consistent with a previous[8] TEM and STM study of Pd clusters. The AFM data, on the other hand, are closer to the Au core results for the C_{12} cluster. The meaning of this result is not clear, but the manner of packing of the clusters in the aggregates in Figure 6 is probably relevant. Perhaps within the aggregates, the alkanethiol chains are interdigitated and/or folded so as to predominantly lie within the plane of the aggregate monolayer.

Solid State Cluster Electronic Conductivities: Temperature and Core−Core Separation Dependencies. This section moves to the electronic properties of the solid state clusters. Application of voltage bias sweeps to IDA fingers covered with films of dry cluster compounds produces current−voltage responses characteristic[12] of electron hopping conductivity, i.e., upwardly curving high-field current *vs* potential, and increasing conductivity with increasing temperature. The cluster electronic conductivity decreases as the number of carbons in the alkanethiolate chains increases, behavior consistent with electron tunneling from Au core-to-core through intervening alkanethiol layers. The following sections present these observations and their analyses.

Low-Voltage, Ohmic Cluster Conductivity. AC-impedance spectra of solid clusters are simple compared to those reported for a similar, ligand-stabilized colloidal system,[11] $Au_{55}(PPh_3)$-Cl_6, in which conductivity spectra implied that electron hopping barriers across *domain boundaries* control the DC conductivity. In contrast, Nyquist plots of AC impedance spectra of solid alkanethiol-stabilized clusters are semicircles reflecting a single, frequency-independent, bulk resistance and capacitance. The AC resistance results were in excellent agreement with those of linear potential sweep methods, which being simpler were generally used.

Using linear potential sweeps in the low voltage region of the current−voltage response, conductivities taken for films on IDA electrodes with small-amplitude sweeps at 30 °C are strongly dependent (Table 5) on the alkanethiolate chain length, falling approximately[13] 10^2-fold for each four-carbon increment: $\sim 10^{-5}$ (C_8 cluster) to $\sim 10^{-7}$ (C_{12} cluster) to $\sim 10^{-9}$ Ω^{-1} cm^{-1} (C_{16} cluster). Considering that the electronic conductivity of Au metal is 4×10^5 Ω^{-1} cm^{-1}, Table 5 results show that

(12) (a) Terrill, R. H.; Sheehan, P. E.; Long, V.; Washburn, S.; Murray, R. W. *J. Phys. Chem.* **1994**, *98(19)*, 5127. (b) Sullivan, M. G.; Murray, R. W. *J. Phys. Chem.* **1994**, *98*, 4343. (c) Jernigan, J. C.; Surridge, N. A.; Zvanut, M. E.; Silver, M.; Murray, R. W. *J. Phys. Chem.* **1989**, *93*, 4620. (d) Surridge, N. A.; Zvanut, M. E.; Keene, R. F.; Sosnoff, C. S.; Silver, M.; Murray, R. W. *J. Phys. Chem.* **1992**, *96*, 962.

(13) The film-to-film scatter in the conductivity data is fairly typical of previous measurements on mixed valent molecular films.[12,14] Variations in conductivity are uncorrelated with those in film thickness. Annealing at elevated temperature (~100 °C) and cycling over the thermal transitions (Figure 7) does not cause significant decay (or enhancement) of film conductivities, but solvent-casting of additional cluster compound over an existing film dramatically decreased conductance on one occasion, so solvent-casting artifacts may be important.

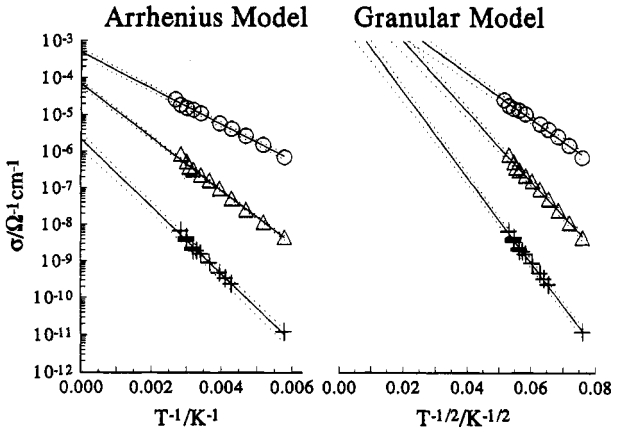

Figure 8. Arrhenius (T^{-1}) and granular model ($T^{-1/2}$) plots of electronic conductivity of the C_8 cluster, (○, $\Delta G^{\ddagger} = 9.1$, $C_o = 40$ kj/mol), the C_{12} cluster (△, $\Delta G^{\ddagger} = 14$, $C_o = 100$ kJ/mol), and the C_{16} cluster (+, $\Delta G^{\ddagger} = 17$, $C_o = 150$ kJ/mol). In vacuo, −100 to +100 °C. C_{16} slope data are from −100 to +20 °C.

the intervening alkanethiol monolayers are potent barriers to electron transfers between the Au cores.

If ample time is allowed in traversing the thermal transitions (Figure 7), the cluster conductivities display[15] linear Arrhenius activation plots ($\ln(\sigma)$ *vs* T^{-1} , Figure 8). The three cluster compounds exhibit different activation barrier energies (Figure 8) and infinite temperature intercepts (Table 5). The activation barrier energies are 9.6 ± 0.6, 16 ± 3 and 19 ± 2 kJ/mol for the C_8, C_{12}, and C_{16} clusters, respectively.

Granular metal, or cermet, theory[16] provides a physical model applicable to the conductivity *vs* temperature data. In the granular metal model, thermal activation is the energy cost, or charging energy, E_{ET}, of an electron transfer between neutral particles to generate a positive and negative pair.[17] The expected temperature dependence of cermet conductivity has the form $\sigma \propto \exp(-E_{ET}/RT)^{1/2}$. Plots of alkanethiol cluster conductivities as $\ln(\sigma)$ *vs* $T^{-1/2}$ are linear, but *not more so* (within error) than are the Arrhenius plots (Figure 8), so the linearity neither impeaches nor validates the granular model. More useful are comparisons of theoretical and experimental determinations of E_{ET}, the former is given by the approximate equation[16]

$$E_{ET} = \frac{N_A e^2 \delta_{EDGE}}{\epsilon_s \epsilon_o 2R_{CORE}[R_{CORE} + \delta_{EDGE}]} \qquad (9)$$

where N_A is Avogadro's number, e the electronic charge, δ_{EDGE} the edge-to-edge gold core separation (Table 3), ϵ_s the static dielectric constant of the intervening matrix, and ϵ_o the permittivity of free space. The E_{ET} derived from a $\ln(\sigma)$ *vs* $T^{-1/2}$ plot, 171 ± 96 kJ/mol, for the C_{12} cluster exactly matches the C_{12}-cluster charging energy calculated with eq 9 if ϵ_s is assumed to be 2.2, a reasonable value between that of dodecane ($\epsilon_s = 2$) and decanol ($\epsilon_s = 5$). To similarly match the E_{ET} values for the C_8 and C_{16} clusters requires ϵ_s, values for the intervening of 5.4 and 1.7, respectively. The dielectric properties of clusters with longer alkanethiol chains are more hydrocarbon-like, which is a reasonable result. Figure 9 plots observed (♦) and theoretical (—) charging energy (E_{ET}) *vs* interparticle separation, δ_{EDGE}, values. The solid lines in Figure 9 are calculated from eq 9, employing dielectric constants which give exact agreement with the observed charging energies ($\epsilon_{C8} = 1.7$, $\epsilon_{C12} = 2.2$, $\epsilon_{C16} = 5.4$). The *trend* observed in the experimental charging energy, increasing with increasing alkanethiol chain length, is qualitatively consistent with the δ_{EDGE} dependency of eq 9.

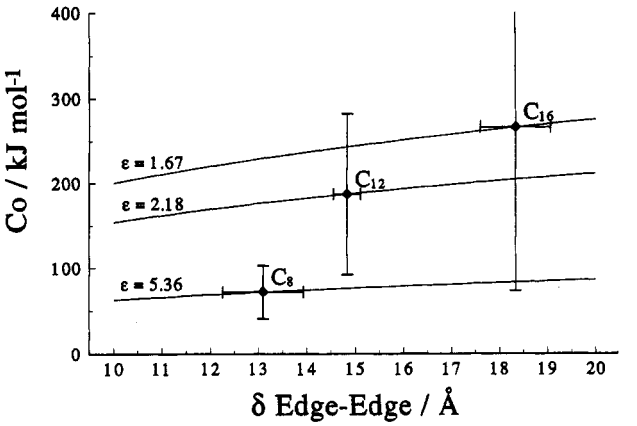

Figure 9. Experimental (♦) and theoretical (solid lines, Equation 9) charging energy (E_{ET}) versus edge−edge interparticle separation.

The distance dependency of electron transfers between Au cores is an especially interesting aspect of the conductivity results, since the alkanethiol chain length ostensibly thereby influences the electronic properties of the cluster compounds. Electron transfer rates are expected[17] to decrease exponentially with distance; for an *all-trans* alkane barrier the decay constant (β) is about 1 Å^{-1}. The complication in the distance dependence caused by the differing activation energies observed for the three chain lengths in the clusters can be handled by extrapolating the linear Arrhenius plots (Figure 8,left) to $(T)^{-1} = 0$, assuming the simple model equation[18]

$$\sigma(T,\delta) = \sigma_0 e^{-\delta_{EDGE}\beta} e^{-\Delta G^{\ddagger}/RT} \qquad (10)$$

where σ is electronic conductivity, β the electron transfer coupling coefficient,[17] and $\Delta G^{\ddagger}$ the activation energy for the electron hop. For each cluster, extrapolating a plot of $\ln(\sigma)$ *vs* T^{-1} gives an intercept $\{\ln(\sigma_0) - \delta/\beta\}$, which plotted *vs* alkanethiol barrier length should have a slope of $-\beta$. Extrapolations in Figure 8 to $(T)^{-1} = 0$ intercepts give infinite temperature conductivities (Table 5) for the C_8, C_{12}, and C_{16} clusters that are (Figure 10) plotted against density-derived edge−edge core spacings (Table 4). Although data for additional alkanethiol chain lengths is ultimately desirable, the Figure 10 linearity is gratifying and supports the reasonableness of the electron tunneling picture. The slope of Figure 10 gives an electron coupling term of 1.2 Å^{-1} (distance normal to the Au core surface) quite close to that reported by others (*ca.* 1

(14) Contact resistance, as evidenced by curved or hysteretical *I/V* plots and/or additional series resistance in the AC impedance spectra, was not significant. Contact resistance was occasionally seen, by AC impedance, when employing Pt IDA electrodes with the C_{16} cluster and once with the C_{12} cluster.

(15) The C_{16} cluster evidenced a change in electrical properties when warmed above *ca.* 20 °C, where activation plots often began to curve upward, current−potential curves taken at high electrical fields to exhibit hysteresis, and conductance to exhibit a slow drift, varying by a few percent over the course of several hours as measured by periodic potential sweeps. These effects for the C_{16} cluster correlate with the temperature of its melting transition seen by DSC. For the activation plots, the thermal equilibration time was judged by the drift in conductivity, and data were recorded when drift was less than 0.1% per minute, typically 10 min.

(16) (a) Abeles, B.; Sheng, P.; Coutts, M. D.; Arie, Y. *Adv. Phys.* **1975**, *24*, 407. (b) Sheng, P.; Abeles, B.; Arie, Y. *Phys. Rev. Lett.* **1973**, *31*, 44.

(17) (a) Newton, M. D. *Chem. Rev.* **1991**, *91*, 767. (b) Hake, R.; McLendon, G. *Chem. Rev.* **1992**, *92*, 481. (c) Guarr, T.; McLendon, G. *Coord. Chem. Rev.* **1985**, *68*, 1. (d) Stein, C. A.; Lewis, N. A.; Seitz, G. *J. Am. Chem. Soc.* **1982**, *104*, 2596.

(18) (a) Plots of $\ln(\sigma)$ vs $T^{-1/2}$, i.e., the cermet model, have much larger uncertainties in their infinite temperature intercepts, and are not useful in this analysis. (b) In electron hopping conduction models more strictly based on eq 10, $\ln(\sigma T)$ *vs* T^{-1} should be plotted. The result in the version of Figure 8 is a 5−10% increase in slope, equally linear plots, and identical β values in a plot like Figure 10.

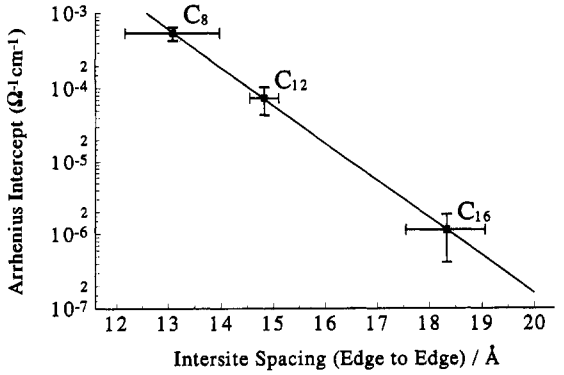

Figure 10. Arrhenius activation plot intercepts ($T^{-1} = 0$) (Ω^{-1} cm^{-1}) plotted versus the Au core edge−edge spacing, assuming all Au cores are 11.9 Å radius and employing a simple cubic packing model. The slope of the plot gives $\beta = 1.18$ Å^{-1}. Error bars are 2σ (95% confidence) based on results from three (C_8), three (C_{12}), and two (C_{16}) density measurements and two (C_8), four (C_{12}), and three (C_{16}) Arrhenius plots.

Å^{-1}) for intermolecular electron transfer through rigid σ bridges[17] and for organized, planar alkanethiol monolayers.[1a,19]

Finally, extrapolation of Figure 10 to zero edge−edge spacing gives a conductivity for, ostensibly, Au cores that are in contact. This conductivity, 1.1×10^3 Ω^{-1} cm^{-1}, lies within two orders of magnitude of that of pure, bulk Au, 4×10^5 Ω^{-1} cm^{-1}. Considering the steric uncertainties, this is a somewhat remarkable correspondence.

High-Field Current−Voltage Curves. Current−potential curves taken at higher voltages (higher free energy gradients) exhibit curvature as shown in Figure 11 and are analyzed with a modification of a bimolecular electron self-exchange relation employed for solid state electron hopping in previous investigations[15]

$$i = \frac{FA\delta_{CORE}C_{NEUTRAL}C_{\pm}k_{EX}}{6}\left(e^{\varrho F\delta_{CORE}\Delta E/2dRT} - e^{-\varrho F\delta_{CORE}\Delta E/2dRT}\right) \quad (11)$$

where

$$C_{\pm} = 2C_{NEUTRAL}e^{-\Delta G_{\pm}/RT} \approx 2C_{NEUTRAL}e^{-\Delta G_{OBSERVED}/RT}$$

where d is the thickness of the cluster layer sandwiched between the IDA electrode finger walls (i.e., the IDA gap size), A the contacting electrode area (IDA wall area, 2×10^{-4} cm^2), $C_{NEUTRAL}$ and $C_{\pm}$ the concentrations of neutral (Table 4) and charged cluster particles, respectively, ρk_{EX} the electron/hole self-exchange rate constant for the clusters, ΔE the applied bias, ρ a fitting parameter which is employed because the current−voltage curves rise more steeply than Marcus[20] theory predicts (and is thought to reflect kinetic dispersity[12a]), and δ_{CORE} the intersite distance (Table 4). The RHS terms in eq 11 represent electrical gradient downfield and upfield electron hops; accounting for both is necessary because, although the overall potential gradient $\Delta E/d$ is large, the intersite gradient $\Delta E\delta_{CORE}/d$ is small. For example, for $\delta_{CORE} = 3$ nm and $\Delta E/d = 10^5$V/cm, the intersite driving force is only 30 mV, or about kT_{298}.

Figure 11, bottom, illustrates the −60° current−voltage responses of films of the three solid cluster compounds, to which eq 11 was fit (see legend). The current sensitivities are scaled

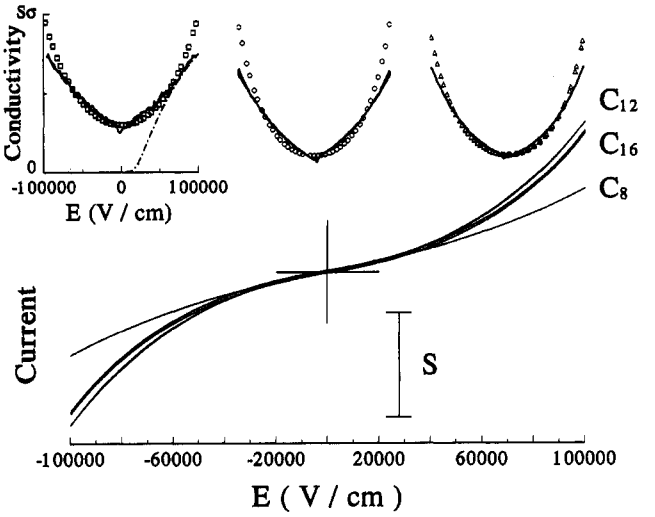

Figure 11. High-field potential sweeps (±50 V, ±10^5 V/cm, 0.1 V/s) of the dry cluster phases at −60 °C on gold IDA electrodes with a 3 μm finger and 5 μm gaps and under vacuum. Experimental data are solid lines. Current sensitivity $S = 1.2$ (C_8), 1.17×10^{-3} (C_{12}), and 8.53×10^{-5} (C_{16},) A/cm^2. For this experiment, the best fit rate constants (eq 11) expressed as the product $\rho C_{\pm}k_{EX}$ are 2.1×10^6, 2.4×10^4, and 1.1×10^2 s^{-1}, the fitting parameter ρ was 1.9, 2.7, and 2.1, and the absolute sums of the residuals are 2.7, 6.8, and 4.6%, for the C_8, C_{12}, and C_{16} clusters, respectively. The topmost panels show the conductivity as a function of field strength (the derivative of the three experimental curves, - - -) and the fits (□, ○, △). The scale on the left applies to all three topmost panels with $S\sigma = 5 \times 10^{-5}$ (C_8), 1.5×10^{-7} (C_{12}), and 1×10^{-8} (C_{16}) Ω^{-1} cm^{-1}.

so that the linear portion of the responses coincide, which accentuates the greater curvature in **I−V** behavior exhibited by the C_{16} and C_{12} clusters relative to the C_8 cluster. The increase in high-field curvature at longer chain length reflects the increasing intersite spacing, δ_{CORE} (exponential terms of eq 11). Increasing high-field curvature also occurs at lowered temperatures. The curves in Figure 11 were fit using eq 11; Table 5, right-hand side, summarizes results for $\rho C_{\pm}k_{EX}$, ρ, and the goodness of fit of eq 11 to C_8, C_{12}, and C_{16} cluster film current−potential curves in the ±100 °C temperature range.

The product $\rho C_{\pm}k_{EX}$ in Table 5 represents[21] the first order (s^{-1}) electron hopping rate constant between Au cores. It would be interesting to estimate the rate of electron hopping in bimolecular terms (i.e., the self-exchange reaction of an electron or hole hopping between Au cores, $Au^0 + Au^- \rightleftarrows Au^- + Au^0$). Estimating the electron hopping rate constant ρk_{EX} in bimolecular terms requires an evaluation of the equilibrium carrier concentration, i.e., of charged clusters ($C_{\pm}$). The carrier concentrations were approximated using a Boltzmann expression, assuming that the experimental activation energy derived from the Arrhenius analysis is that required to produce carriers. The tiny (*ca.* 1 part in 10^4 at room temperature for C_{12}) concentration of charged particles $C_{\pm}$ depletes the concentration $C_{NEUTRAL}$ insignificantly. The average electron transfer rate constants[22] between cluster cores based on these assumptions are[23] 2×10^{10}, 7×10^8, and 2×10^8 M^{-1} s^{-1} for C_8, C_{12}, and C_{16} clusters, respectively. These highly approximate rate

(19) Carter, M. T.; Rowe, G. K.; Richardson, J. N.; Tender, L. M.; Terrill, R. H.; Murray, R. W. *J. Am. Chem. Soc.* **1995**, *117*, 2896.

(20) (a) Marcus, R. A.; Sutin, N. *Biochim. Biophys. Acta* **1985**, *109*, 1738−1745. (b) Marcus R. A. *Annu. Rev. Phys. Chem.* **1964**, *15*, 155. (c) Marcus R. A. *J. Chem. Phys.* **1965**, *43*, 1965. (d) Marcus R. A. *Discuss. Faraday Soc.* **1960**, *29*, 21.

(21) The fitting factor is included in the product since previous[12a,b] solid state electron transport measurements comparing results from eq 11 with other techniques that are insensitive to kinetic dispersion have taught us that the product ρk_{EX} is a better representation of an "average" rate constant in a dispersive situation.

(22) The rate constant k_{EX} derived from applying this approximation to experimental data is temperature independent because we cannot separate formation from transport of carriers, and so all temperature dependence of conductivity is placed into changes in carrier concentration, not carrier hopping rate.

constants (given the assumptions involved in estimating the carrier concentrations) suggest that the mobilities of electrons and holes in the solid cluster are quite high.

Finally, we should note that although eq 11 fits the high-field current−potential curves fairly well, systematic deviations can be detected in the fits. The topmost insets in Figure 11 show the conductivity *vs* field strength that is observed (−) and that is predicted by eq 11 (□, C_8; ○, C_{12}; △, C_{16}). The deviations for the C_8 cluster conductivity seem more pronounced. The significance of these deviations remains to further investigation of this interesting form of electronic conductivity. It is worth noting that the uncertainty in the meaning of the high-field results generates only modest uncertainty in the *rate constant* estimates since the rate constant $\rho C_{\pm} k_{EX}$ can be alternatively evaluated from the ohmic conductivity regime of the current−potential curve alone, and the data in Table 5 would change little or not at all.

(23) Expressing these results in different units gives carrier diffusion coefficients of 2×10^{-5}, 7×10^{-6}, and 6×10^{-7} cm^2/s and mobilities of 8×10^{-4}, 3×10^{-4}, and 2×10^{-5} $cm^2\ V^{-1}\ s^{-1}$ for C_8, C_{12}, and C_{16}, respectively.

Acknowledgment. This work was supported by grants from the National Science Foundation and the Department of Energy. The authors wish to acknowledge Nippon Telegraph and Telephone company for the generous gift of interdigitated array electrodes. Access to DSC equipment was provided by Professor J. DeSimone. The research at Oak Ridge National Laboratories is supported by the Division of Materials Sciences, U.S. Department of Energy under contract No. DE-AC05-84OR21400 with Martin Marietta Energy Systems Inc.

JA952416W